AGU PUBLICATIONS

Geophysical Research Letters

RESEARCH LETTER
10.1002/2017GL073633

Key Points:
- Idealized global warming experiments show enhanced poleward motion of individual cyclonic storms
- A PV tendency analysis of the cyclone composites reveals two dominant mechanisms: increased nonlinear advection and latent heat release
- Enhanced poleward motion of storms could imply a poleward shift and a more poleward deflected shape of localized storm tracks

Supporting Information:
- Figure S1
- Figure S2
- Figure S3
- Supporting Information S1

Correspondence to:
T. Tamarin,
talia.tamarin@weizmann.ac.il

Citation:
Tamarin, T., and Y. Kaspi (2017), The poleward shift of storm tracks under global warming: A Lagrangian perspective, *Geophys. Res. Lett.*, *44*, 10,666–10,674, doi:10.1002/2017GL073633.

Received 28 MAR 2017
Accepted 27 APR 2017
Published online 18 OCT 2017

The poleward shift of storm tracks under global warming: A Lagrangian perspective

T. Tamarin[1] **and Y. Kaspi**[1]

[1] Department of Earth and Planetary Sciences, Weizmann Institute of Science, Rehovot, Israel

Abstract Comprehensive models of climate change projections have shown that the latitudinal band of extratropical storms will likely shift poleward under global warming. Here we study this poleward shift from a Lagrangian storm perspective, through simulations with an idealized general circulation model. By employing a feature tracking technique to identify the storms, we demonstrate that the poleward motion of individual cyclones increases with increasing global mean temperature. A potential vorticity tendency analysis of the cyclone composites highlights two leading mechanisms responsible for enhanced poleward motion: nonlinear horizontal advection and diabatic heating associated with latent heat release. Our results imply that for a 4 K rise in the global mean surface temperature, the mean poleward displacement of cyclones increases by about 0.85° of latitude, and this occurs in addition to a poleward shift of about 0.6° in their mean genesis latitude. Changes in cyclone tracks may have a significant impact on midlatitude climate, especially in localized storm tracks such as the Atlantic and Pacific storm tracks, which may exhibit a more poleward deflected shape.

1. Introduction

Traditionally, two complementary approaches are used to study the midlatitude storm tracks and the mobile weather systems that compose them. In the Eulerian approach, storm tracks are defined as regions of enhanced eddy kinetic energy (EKE) [*Blackmon et al.*, 1977] (Figure 1), where eddies are defined as transient variations with a typical time scale of 3–10 days. In the Lagrangian approach, these regions are defined as aggregates of tracks of individual storms, thus historically named "storm tracks." The latter approach requires a Lagrangian feature tracking of the storms to analyze their statistical distributions [e.g., *Hodges*, 1995].

Understanding how the storm tracks respond to climate change, and how that may influence our climate and weather, is of major importance. Previous studies using climate change projection models have shown that the mean intensity of cyclones is likely to increase and the total number of cyclones to decrease, though the number of extreme cyclones could potentially increase [*Lambert and Fyfe*, 2006; *Ulbrich et al.*, 2008; *Bengtsson et al.*, 2009; *Zappa et al.*, 2013]. In addition, the storm tracks and the corresponding maximum of EKE are likely to expand upward and shift poleward as a result of climate change [*Yin*, 2005; *Bengtsson et al.*, 2006; *Ulbrich et al.*, 2008; *Bengtsson et al.*, 2009; *Wu et al.*, 2011; *Chang et al.*, 2012], and the latter is especially clear in the Southern Hemisphere (SH) [*Chang et al.*, 2012] (Figure 1).

The poleward shift of the storm tracks was found both in reanalysis data of recent years [*Fyfe*, 2003; *Son et al.*, 2008] and in multimean ensemble projections of models forced with enhanced greenhouse gas concentrations [*Yin*, 2005; *Bengtsson et al.*, 2006; *Ulbrich et al.*, 2008; *Bengtsson et al.*, 2009; *Chang et al.*, 2012; *Barnes and Polvani*, 2013]. The latter suggest that the storm tracks will shift on average between 1° and 2° in latitude poleward under a CO_2 doubling scenario [*Chang et al.*, 2012]. Several mechanisms have been proposed to explain the poleward shift, including changes in the meridional location of maximum baroclinicity [*Yin*, 2005], increased static stability in the subtropics and midlatitudes [*Lu et al.*, 2007, 2010], increased tropical convective stability [*Mbengue and Schneider*, 2013], enhanced upper level tropical heating [*Butler et al.*, 2010], increased sea surface temperatures [*Caballero*, 2005; *Kodama and Iwasaki*, 2009; *Graff and LaCasce*, 2014], and changes in eddy characteristics [*Kushner and Polvani*, 2006; *Chen and Held*, 2007; *Lorenz and DeWeaver*, 2007; *Kidston et al.*, 2010; *Riviére*, 2011]. However, there is currently no agreement on what is the dominant dynamical process responsible for the poleward shift.

The complexity of the climate system, along with its internal variability, nonlinear feedbacks, and dynamical processes, often makes it extremely hard to identify the governing underlying mechanisms. Our ability to

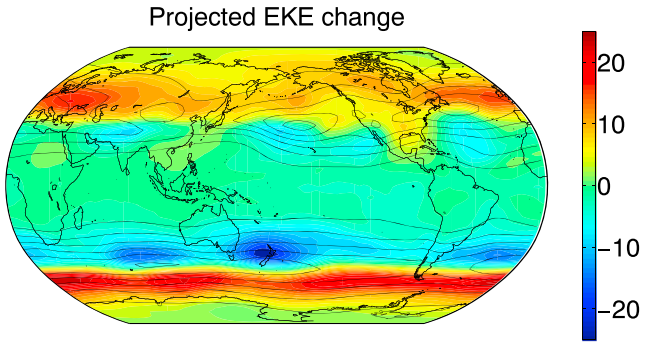

Figure 1. Eddy kinetic energy ($m^2\ s^{-2}$) at 300 hPa in current climatology (black contours) and the projected change (the last 20 years of the 21st century minus the last 20 years of the twentieth century) (colors), from all models participating in Phase 5 of the Coupled Model Intercomparison Project (CMIP5) in the high emissions Representative Concentration Pathway 8.5 scenario, for a NH winter (December–February).

simulate the global circulation is increasingly improving, as a result of collective efforts to improve both the parameterizations of unresolved processes and the numerical resolution. However, large model biases and uncertainties for climate change projections are still obtained. For these reasons, there is need for more idealized and simplified studies, where the full global circulation models are stripped to retain only the most basic elements. In this study, such a simplified approach is taken to study the poleward shift of the storm tracks.

This is done by performing global warming experiments in an idealized zonally symmetric general circulation model (GCM), by systematically increasing the global mean surface temperature. The model has simplified radiative transfer and moist convection schemes [*Frierson et al.*, 2006; *O'Gorman and Schneider*, 2008], and it is an aquaplanet model. It does not include, for example, continents, clouds, sea ice, and chemical processes. Yet the poleward shift of cyclones with global warming is well captured in our model. The lack of local asymmetries results in a climate that resembles more the SH storm track on Earth (Figure 1), and our analysis is therefore more adequate for explaining the SH shift of the storm tracks. In the Northern Hemisphere (NH), the presence of continents results in a localized storm track that is deflected poleward [*Brayshaw et al.*, 2008; *Kaspi and Schneider*, 2013], and a more pronounced poleward motion of cyclones occurs in these regions. However, the basic mechanisms for poleward propagation of cyclones in a zonally symmetric storm track, which are shown to intensify in a warmer climate, are also relevant for the NH [*Tamarin and Kaspi*, 2017a]. This implies that the Atlantic and Pacific storm tracks in the NH may become more deflected poleward under a global warming scenario.

In this study a Lagrangian perspective is adopted to study the poleward shift, by employing a feature tracking technique [*Hodges*, 1995] and considering dynamics at the storm scale. This is different than most previous studies, which examined the poleward shift of the storm track from an Eularian perspective, as a whole. The vorticity data are used to track cyclones and construct composites of the potential vorticity (PV) tendencies associated with them. Thus, the dominant terms in the PV tendency analysis can be easily interpreted. It is shown that horizontal advection associated with the nonlinear self-advection of the cyclones, as well as the PV tendency due to diabatic processes associated with latent heat release (LHR), both contribute to the poleward motion of the cyclone. These mechanisms are then shown to intensify in a warmer climate.

The main goal of this paper is to present a new perspective on the poleward shift that explains it qualitatively, rather than to give an exact prediction for the shift. The real world is obviously far more complicated than the idealized GCM used here, as there are many important processes that are neglected (e.g., continents, topography, clouds, and sea ice). However, the fact that a poleward shift is obtained even in such a simplified model indicates that there is a more basic underlying dynamical mechanism. The idealized GCM therefore serves to develop a better understanding of the process and to highlight the important signals that can then be identified in more complicated and realistic models [*Tamarin and Kaspi*, 2017b].

2. Methods

2.1. Idealized GCM

The idealized GCM uses the spectral core of Geophysical Fluid Dynamics Laboratory Flexible Modeling System and solves the hydrostatic primitive equations for an ideal-gas atmosphere [*Frierson et al.*, 2006; *O'Gorman and Schneider*, 2008]. It is a three-dimensional model with spherical geometry and a lower layer of a slab ocean. The horizontal resolution used for this study is T85 (1.4° × 1.4°), and the vertical coordinate $\sigma = p/p_s$ (where p_s is the surface pressure and p is pressure) has 30 levels.

The idealized GCM has a simplified representation of water vapor, perpetual equinox conditions, and a simplified two-stream gray radiation scheme [*Frierson et al.*, 2006], where longwave optical thickness τ depends only on pressure and latitude:

$$\tau = \left[f_l\sigma + \left(1 - f_l\right)\sigma^4\right]\left[\tau_e + \left(\tau_p - \tau_e\right)\sin^2\phi\right]. \quad (1)$$

Here ϕ is latitude, $f_l = 0.2$, and $\tau_e = 8.2$, $\tau_p = 2.4$, are the longwave optical thicknesses at the equator and pole, respectively, chosen to roughly mimic the temperature distribution on Earth. The model has simplified moist convection and condensation schemes [*Frierson et al.*, 2006], and water vapor is relaxed toward a fixed relative humidity. In addition, a planetary boundary layer scheme determines the surface temperature through an energy balance that includes thermal radiation, latent heat, and sensible heat.

2.2. Storm Tracking Algorithm and Composites

An objective feature point identification and tracking technique [*Hodges*, 1995] is used to identify cyclones and track them. In this study, we use the 780 hPa vorticity field to identify the cyclones, and their centres are then tracked every 6 h (similar results are obtained when the 850 hPa level is used instead). A filtering of the data is performed prior to the tracking, to reduce noise, and the data are smoothed to a T42 grid [*Hodges*, 1995, 1999]. The background flow is also removed to isolate the synoptic and mesoscale features. A cutoff of 10^{-5} s^{-1} is used for the vorticity field, and only cyclones that travel more than 1000 km and for more than 2 days are used for the analysis.

Next, the tracks are used to produce cyclone composites. For each cyclone identified, we place a box around its center (30° latitude by 40° longitude). The composites are computed during the growth stage, until the time of maximum intensity of each cyclonic storm, and then averaged over all of them. We use the 1500 strongest cyclones from each 3000 simulation days for each run, out of approximately 17,000 cyclones identified in the coldest experiment and 15,000 in the warmest experiment (the total number of cyclones identified decreases with the warming). However, similar qualitative results are obtained if more cyclones are considered for the analysis (see supporting information Figure S3).

2.3. Idealized Global Warming Experiments

The global warming experiments are performed in the idealized GCM by increasing the optical depth parameters at the equator and the pole [e.g., *O'Gorman and Schneider*, 2008; *Levine and Schneider*, 2011; *Pfahl et al.*, 2015]. A reference simulation is used, with parameters of the longwave optical thicknesses at the equator and pole chosen to reproduce a meridional temperature similar to that on Earth, as given in equation (1). An additional 11 simulations are then performed where the optical depths at the equator and the poles are multiplied by the same constant α, where $1 \leq \alpha \leq 1.85$. This results with a gradual increase in the global mean surface temperatures, of up to 298.2 K.

3. Poleward Motion of Cyclones

The tracks of the 1500 most intense storms, over a period of 3000 days, are shown for a simulation with conditions similar to current Earth's conditions ($T_s = 286.8$, Figure 2a). The tracks are computed using the vorticity field at 780 hPa, where color indicates the intensity of the storm (normalized by 10^{-5} s^{-1}), and translated to start from a common point. The level of 780 hPa is chosen here as representative of the lower level, but the results are essentially identical if the 850 hPa level is used instead. Only tracks originating in the midlatitudes (between latitude 30° and 60°) are considered, and tracking is performed only during the growth stage of the cyclones. The mean cyclonic system propagates approximately 10.2° in latitude poleward and 46.6° in longitude eastward (the black arrow in Figure 2a). The latitudinal displacement found here is similar to the mean latitudinal displacement of the SH storm track from NCEP reanalysis data, for the years 1980–2013 (see supporting information Figure S1).

To understand the mechanisms responsible for the poleward motion of cyclones and how they may vary in a warmer climate, we analyze the dynamics from a PV perspective. PV, which is a measure for the absolute circulation of an air parcel that is enclosed between two surfaces of constant potential temperature, is a very useful concept in geophysical fluid dynamics [*Pedlosky*, 1987]. Following an air parcel, PV is conserved for an adiabatic and inviscid process. The Ertel PV, written in pressure coordinates, is given by

$$q = -g\left(f\hat{k} + \vec{\nabla}_p \times \vec{u}\right) \cdot \vec{\nabla}_p\theta, \quad (2)$$

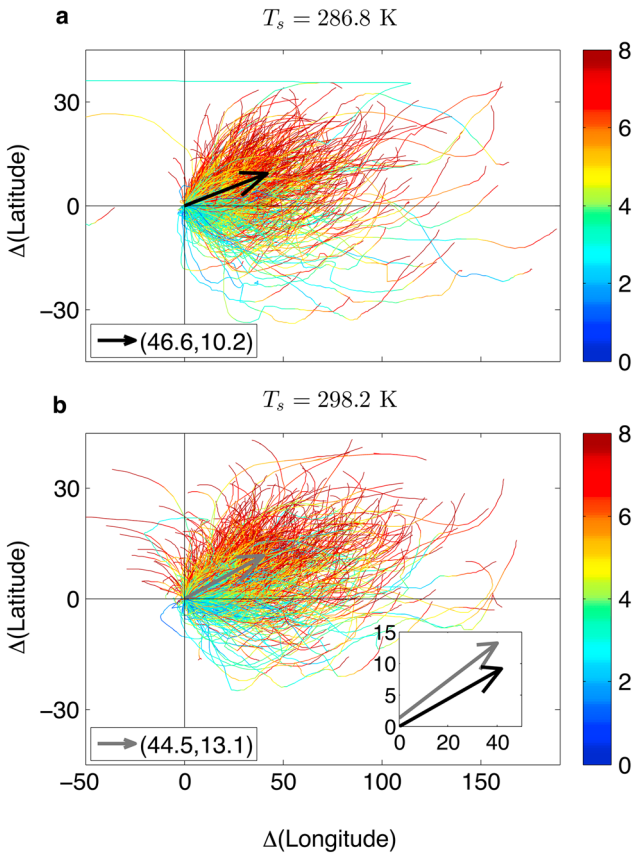

Figure 2. Tracks of the low-level cyclones (780 hPa), translated to a common starting point, for a global mean surface temperature of (a) $T_s = 286.8$ K and (b) $T_s = 298.2$ K. The tracks are plotted until the cyclones reach their maximum intensity, where color indicates the intensity of the vorticity anomaly (scaled by 10^{-5} s^{-1}). The black arrow in Figures 2a and the grey arrow in 2b show the mean displacement vector of the cyclones, and the legend indicates the mean displacement in the longitudinal and latitudinal directions, respectively. The small box in Figure 2b shows the two displacement arrows superimposed together, where the black arrow of the coldest simulation starts from the origin and the grey arrow of the warmest simulation is shifted poleward by an amount equal to the mean shift of the starting latitude of cyclones between the two simulations (1.3°).

where f is the planetary vorticity, θ is the potential temperature, and $\vec{\nabla}_p \times \vec{u}$ is the relative vorticity, and satisfies

$$\frac{\partial q}{\partial t} = -\vec{u} \cdot \vec{\nabla} q - \omega \frac{\partial q}{\partial p} + Q. \quad (3)$$

Here $\mathbf{u} = (u, v)$ are the velocities in the zonal and meridional directions, respectively, $\omega = \frac{dp}{dt}$ (vertical velocity in pressure coordinates), and $\vec{\nabla} = (\frac{\partial}{R\cos\theta\partial\phi}, \frac{\partial}{R\partial\theta})$, where R is the radius of Earth and ϕ and θ are the zonal and meridional coordinates, respectively. The last term represents diabatic processes such as latent heat release, given by

$$Q = -g\left(f\hat{k} + \vec{\nabla}_p \times \vec{u}\right) \cdot \vec{\nabla}_p \left(\frac{\mathrm{d}\theta}{\mathrm{d}t}\right). \quad (4)$$

Note that at the level considered here (780 hPa) the surface drag is small and was therefore not included in the analysis. To specifically calculate the contribution of latent heat release, we use the expression derived by *Emanuel et al.* [1987]:

$$\left(\frac{\mathrm{d}\theta}{\mathrm{d}t}\right)_{\mathrm{LHR}} = \omega\left(\frac{\partial\theta}{\partial p} - \frac{\gamma_m}{\gamma_d}\frac{\theta}{\theta_E}\frac{\partial\theta_E}{\partial p}\right). \quad (5)$$

Here θ_E denotes equivalent potential temperature, and γ_d, γ_m represent the dry and moist lapse rates, respectively. In the absence of moist processes $\gamma_m = \gamma_d$, $\theta = \theta_E$, and hence $\left(\frac{\mathrm{d}\theta}{\mathrm{d}t}\right)_{\mathrm{LHR}} = 0$.

A composite of the low-level (780 hPa) PV associated with these cyclones, during their growth stage, is shown in Figures 3a–3c. The PV analysis reveals two dominant mechanisms responsible for their poleward tendency. The first term on the right-hand side of equation (3), the horizontal advection of the perturbation PV, contributes to a positive PV tendency on the northeastern side of the anomaly and a negative PV tendency on the southwestern side of the cyclone (Figure 3a). A decomposition of this term to its different components (not shown) shows that it is the zonal flow that is responsible for the eastward advection of the perturbation PV, while the nonlinear advection terms are those responsible for the poleward tendency [*Tamarin and Kaspi*, 2016]. This poleward advection is associated with lower level winds induced by PV at upper levels [*Gilet et al.*, 2009; *Oruba et al.*, 2013; *Coronel et al.*, 2015; *Tamarin and Kaspi*, 2016]. In the PV perspective, cyclogenesis is described as the mutual amplification of a positive low-level PV anomaly, associated with the cyclone, and a positive upper level PV anomaly to its west [*Bretherton*, 1966; *Hoskins et al.*, 1985]. During the growth stage of the cyclone, the fact that the lower level PV is to the east of the upper level PV implies that it resides in a region where the upper level wind is oriented poleward. Thus, a poleward wind is induced at low levels, advecting the low-level PV poleward. This was demonstrated in *Tamarin and Kaspi* [2016] using PV inversion, which showed explicitly that the poleward advection of the low-level cyclones is a result of wind induced by the upper levels.

The second mechanism found for the poleward motion of the low-level PV is associated with diabatic warming due to latent heat release (Figure 3b). Since cyclonic circulation in the NH (SH) is anticlockwise (clockwise),

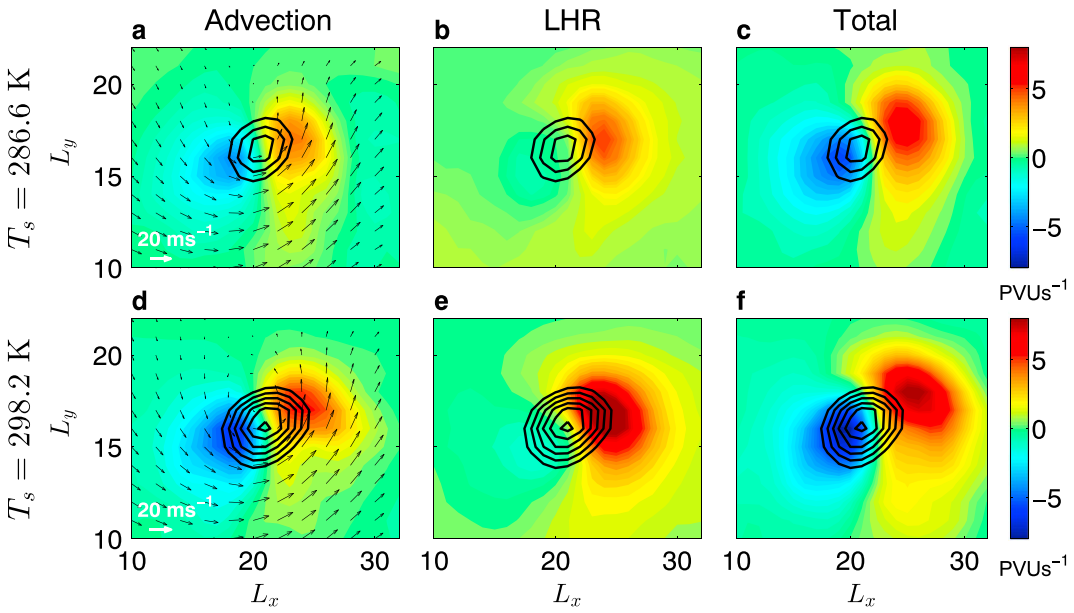

Figure 3. Cyclone composites of low-level (780 hPa) PV tendency from (a and d) horizontal PV advection by low-level winds (black arrows) and (b and e) diabatic heating due to latent heat release. (c and f) Total PV tendency ($\frac{\partial q'}{\partial t}$) at low levels. Figures 3a–3c correspond to a simulation with a global mean surface temperature of $T_s = 286.8$ K and Figures 3d–3f to $T_s = 298.2$ K. PV tendencies are given in units of 10^{-6} PVU s^{-1}. The low-level PV anomaly is shown in black contours, with lowest contour equal to 0.65 PVU and contour intervals of 0.05 potential vorticity unit (PVU), 1 PVU = 10^{-6} (K*m^2)/(kg*s). L_y and L_x are the latitudinal and longitudinal lengths (in degrees) of the composite box, respectively.

it systematically advects low temperatures to the west of the cyclone and high temperatures to its east. This poleward moving moist and warm air to the east of the cyclone also ascends upward, and as it does so it cools and condenses, releasing latent heat. Thus, latent heat release is maximized in the midtroposphere in the northeastern side of the cyclone. Diabatic heating at the middle of the atmosphere can produce a positive low-level PV tendency and a negative upper level PV tendency [*Davis et al.*, 1993; *Stoelinga*, 1996; *Lackmann*, 2002; *Posselt and Martin*, 2004; *Hawcroft et al.*, 2016a]. This occurs because the isentropes above the warming will tend to widen (i.e., $|\frac{\partial \dot{\theta}}{\partial p}|$ decreases), while the isentropes below the warming will tend to narrow (i.e., $|\frac{\partial \dot{\theta}}{\partial p}|$ increases). Hence, from equations (3) and (4), $\frac{dq}{dt} < 0$ at upper levels and $\frac{dq}{dt} > 0$ at lower levels. In addition, the warming enhances the upward motion and therefore the convergence at lower levels, which enhances even further the relative vorticity at low levels. From its definition (equation (2)), the PV therefore increases at low levels and decreases at upper levels. The positive diabatically produced PV tendency at low levels contributes to the northeastward propagation of the low-level cyclone [*Tamarin and Kaspi*, 2016]. The processes associated with latent heating may be especially important for future projections of climate change [*Hawcroft et al.*, 2016a], particularly given the observed biases in precipitation intensity produced by some models [*Hawcroft et al.*, 2016b]. Finally, the total PV tendency (Figure 3c) shows a dipole that is tilted SW-NE, consistent with the overall eastward and poleward propagation of the low-level cyclones.

4. Enhanced Poleward Motion in Warmer Climates

To analyze systematically how the mechanisms described above change when the background climate warms, we perform a series of experiments where we gradually increase the global mean surface temperature. This is achieved by varying the longwave optical thickness at the equator and the pole (by multiplying them by the same constant, see section 2.3), which represents changes in longwave absorbers such as carbon dioxide and water vapor.

In a warmer climate ($T_s = 298.2$, Figure 2b), the mean cyclonic system is not only formed 1.3° in latitude more poleward but also now propagates approximately 13.1° in latitude poleward and 44.5° in longitude eastward until maximum intensity (grey arrow in Figure 2b). Hence, in addition to a shift in the mean starting latitude of the cyclonic storms, their poleward latitudinal drift also increases, and their longitudinal drift slightly

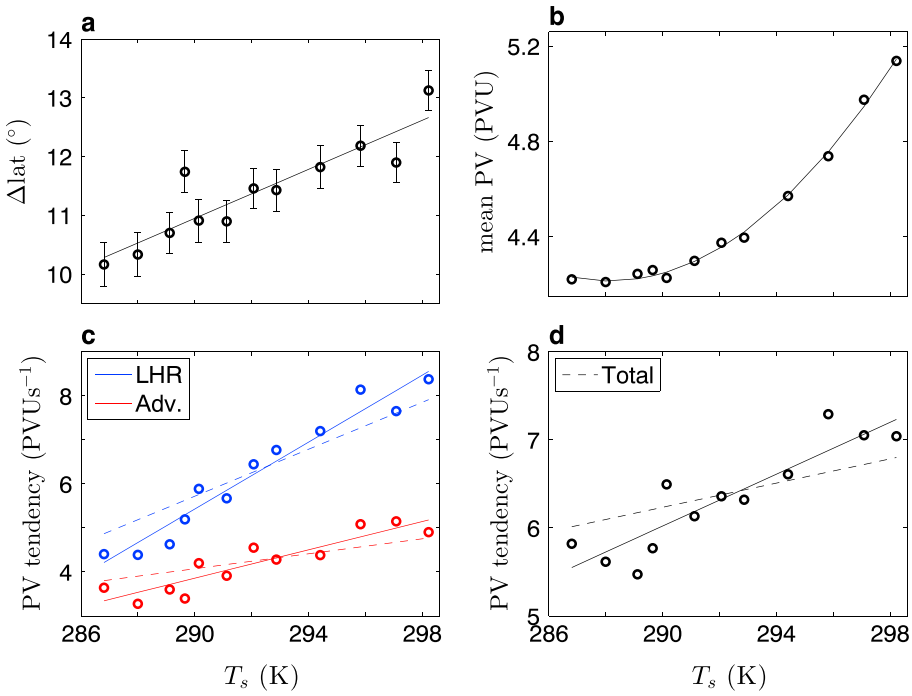

Figure 4. The dependence on the global mean surface temperature (K) of (a) the mean latitudinal displacement of cyclones, until their maximum intensity is reached, (b) the mean intensity of the composite PV perturbation, (c) the mean values of the PV tendencies from the horizontal advection term (red) and diabatic heating associated with latent heat release (blue) from the cyclone composites, and (d) the mean value of the total PV tendency from the cyclone composites. The mean PV and PV tendencies are measured as an average over the grid points surrounding the maximum value. Each dot represents individual run, and the lines show the best linear fit in Figures 4a, 4c, and 4d, while in Figure 4b a quadratic fit is used. Dashed lines in Figures 4c and 4d show the normalized PV tendencies. The error bars in Figure 4a reflect the standard error of the mean latitudinal displacement for each run.

decreases. This implies that the mean track of intensifying cyclonic systems becomes more tilted toward the pole. Both the PV tendency due to the horizontal advection terms (Figure 3d) and the PV production due to latent heat release (Figure 3e) intensify. The total PV tendency in a warmer climate (Figure 3f) results in a stronger motion of the low-level cyclone toward the northeast. The PV tendencies in a warmer simulation appear to be not only stronger but also more SW-NE oriented. This is consistent with the enhanced poleward propagation and overall tilt of the mean cyclonic track in the warmer simulation (Figure 2b).

Gradually warming the background climate shows that the poleward motion of cyclones is enhanced, and the latitudinal distance traveled by the cyclones until maximum intensity increases almost linearly (Figure 4a). The mean starting latitude of the cyclonic storms also gradually shifts poleward, due to expansion of the Hadley Cell and associated shift in maximum baroclinicity [*Lu et al.*, 2007], but does not explain the total observed shift in the latitude of maximum cyclone intensity (see supporting information Figure S2). Hence, the changes in the cyclone displacements are crucial for explaining the overall observed shift. Consistent with the enhanced poleward propagation, both the mean value of the horizontal PV advection (red dots in Figure 4c), and due to latent heat release (blue dots in Figure 4c) increase. In addition, the mean value of the PV perturbation increases (Figure 4b).

The enhancement of the horizontal PV advection in a warmer climate (red dots in Figure 4c) may be related to both the enhancement of the upper level jet (not shown) and the low-level PV perturbation (Figure 4b). Stronger upper level winds imply that the induced poleward velocity at low levels is stronger. Stronger low-level PV anomalies, which are also associated with stronger upper level PV, tend to propagate more poleward.

The increase of the PV tendency associated with latent heat release in a warmer climate (blue dots in Figure 4c) is potentially a result of the Clausius-Clapeyron relation, which implies that a warmer atmosphere has a larger saturation water vapor pressure, given that relative humidity does not change significantly (though there may

be some nontrivial changes in relative humidity associated with changes in advection around the composite cyclone, and moisture availability may be more important locally [*Pfahl and Sprenger*, 2016]). Hence, more latent heat release occurs in a warmer climate, which both intensifies the low-level cyclones and contributes to their poleward propagation. Interestingly, in our model, at temperatures close to Earth's temperatures, the two processes responsible for the poleward propagation appear to be of similar magnitude. However, as the climate warms, latent heat release becomes more dominant (Figure 4c), possibly due to the dependence of saturation vapor pressure on temperature. The change in saturation vapor pressure as the climate warms is especially important, since it influences the precipitation associated with the cyclonic storms. For example, it was found that changes in composite cyclone precipitation intensity in a warmer climate are almost entirely thermodynamically driven (increase in water vapor path) rather than dynamically driven (increase in mean cyclone wind speed) [*Yettella and Kay*, 2016].

The reduction in the longitudinal displacement may be related to the enhancement of the low-level PV anomalies in a warmer climate, as stronger cyclones can also self-propagate faster westward (in a similar manner to the westward propagation mechanism of Rossby waves [*Rossby*, 1948]). In addition, there is a reduction of the zonal mean zonal flow at high latitudes (not shown), and this contributes to the fact that the cyclones propagate less eastward in our idealized global warming experiments but may not be the case in more comprehensive GCMs.

Note that because the cyclone intensity and its associated PV perturbation increase with the mean temperature, looking at the tendencies alone does not necessarily imply a larger poleward motion (since a stronger amplitude would require a stronger tendency in order to propagate). For that reason, the previous analysis was repeated but with PV tendencies normalized by the corresponding mean PV anomaly (dashed lines in Figures 4c and 4d). The results are similar and show the overall increase of the PV tendency with the global mean surface temperature.

5. Discussion and Summary

In this study, it is suggested that the poleward shift of storm tracks in a warmer climate can be viewed as an enhanced poleward motion of individual cyclones. From a Lagrangian storm perspective, two mechanisms are shown to produce a poleward tendency: nonlinear horizontal advection, which is associated with the upper level PV, and PV tendency due to latent heat release. Both are shown to intensify in a warmer climate, which can explain the enhanced latitudinal drift of cyclones. This occurs in addition to other suggested mechanisms that cause a poleward shift, such as the expected poleward shift of the meridional temperature gradient and baroclinic zone due to the expansion of the Hadley cell [e.g., *Yin*, 2005].

Note that in order to obtain a poleward shift in a zonally symmetric storm track, such as in the SH, it is not enough to have a more tilted mean track. Rather, it is the latitudinal displacement that ultimately determines whether a poleward shift is obtained or not. For example, if the mean cyclonic track becomes more tilted, but its lifetime becomes shorter (or if it propagates more slowly), then the overall storm track will not shift poleward. Enhanced latitudinal displacement of cyclones until maximum intensity necessarily implies a poleward shift of the EKE. In a localized storm track such as those observed in the NH, this picture is more complex. A larger latitudinal displacement, given the same mean cyclonic tilt, could just imply a downstream extension of the storm track toward the NE direction. On the contrary, a larger mean cyclonic tilt in a localized storm track implies that the storm track becomes more deflected, but not necessarily a poleward shift of the maximum EKE.

Our results imply that an additional latitudinal drift of 0.21° in latitude will occur for every 1 K of warming (calculated from the slope of a linear best fit of Figure 4a). The longitudinal displacements predict a decrease in longitudinal drift of 0.37° for every degree of warming (not shown). These value are, in fact, sensitive to the intensity and number of cyclones on which the averaging is performed (see supporting information Figure S3). However, they consistently show an increase in the mean latitudinal displacement with warming. In addition, the mean genesis latitude of the cyclones shifts by about 0.15° in latitude poleward per 1 K of warming (see supporting information Figure S2). This implies an overall poleward shift of approximately 1.5° in the latitude of peak cyclone intensity for a global mean surface temperature that is 4 K warmer than the mean temperature today, where more than 50% of this shift is due to the changes in the meridional cyclone displacements (rather than changes in the mean starting latitude alone). Taking into account both the latitudinal and the longitudinal displacements, it is suggested that the tilt of the mean tracks of cyclones is expected

to increase. This implies both a poleward shift of the storm tracks as a whole, and that the localized storm tracks may become more deflected toward the pole. This can have a significant impact on regional climate in the midlatitudes, especially for regions close to the eastern ocean boundaries in the localized storm tracks in the NH.

Notation

PV potential vorticity.
EKE eddy kinetic energy.
LHR latent heat release.
NH Northern Hemisphere.
SH Southern Hemisphere.

Acknowledgments
The authors thank Kevin Hodges for providing the tracking algorithm and his generous help with its implementation. The CMIP5 data used to produce Figure 1 are available at the World Data Center for Climate (WDCC) at http://cera-www.dkrz.de/WDCC/ui/. This research was supported by the Israeli Science Foundation (grant 1819/16).

References

Barnes, E. A., and L. Polvani (2013), Response of the midlatitude jets, and of their variability, to increased greenhouse gases in the CMIP5 Models, *J. Clim.*, *26*, 7117–7135.
Bengtsson, L., K. Hodges, and E. Roeckner (2006), Storm tracks and climate change, *J. Clim.*, *19*(15), 3518–3543.
Bengtsson, L., K. I. Hodges, and N. Keenlyside (2009), Will extratropical storms intensify in a warmer climate?, *J. Clim.*, *22*(9), 2276–2301.
Blackmon, M., J. Wallace, N. Lau, and S. Mullen (1977), An observational study of the Northern Hemisphere wintertime circulation, *J. Atmos. Sci.*, *34*(7), 1040–1053.
Brayshaw, D. J., B. Hoskins, and M. Blackburn (2008), The storm-track response to idealized SST perturbations in an aquaplanet GCM, *J. Atmos. Sci.*, *65*, 2842–2860.
Bretherton, F. P. (1966), Baroclinic instability and the short wavelength cut-off in terms of potential vorticity, *Q. J. R. Meteorol. Soc.*, *92*, 335–345.
Butler, A. H., D. W. J. Thompson, and R. Heikes (2010), The steady-state atmospheric circulation response to climate change-like thermal forcings in a simple general circulation model, *J. Clim.*, *23*, 3474–3496.
Caballero, R. (2005), The dynamic range of poleward energy transport in an atmospheric general circulation model, *Geophys. Res. Lett.*, *32*, L02705, doi:10.1029/2004GL021581.
Chang, E. K. M., Y. Guo, and X. Xia (2012), CMIP5 multimodel ensemble projection of storm track change under global warming, *J. Geophys. Res.*, *117*, D23118, doi:10.1029/2012JD018578.
Chen, G., and I. M. Held (2007), Phase speed spectra and the recent poleward shift of Southern Hemisphere surface westerlies, *Geophys. Res. Lett.*, *34*, L21805, doi:10.1029/2007GL031200.
Coronel, B., D. Ricard, G. Rivière, and P. Arbogast (2015), Role of moist processes in the tracks of idealized mid-latitude surface cyclones, *J. Atmos. Sci.*, *72*, 2979–2996.
Davis, C. A., M. T. Stoelinga, and Y.-H. Kuo (1993), The integrated effect of condensation in numerical simulations of extratropical cyclogenesis, *Mon. Weather Rev.*, *121*, 2309–2330.
Emanuel, K., M. Fantini, and A. Thorpe (1987), Baroclinic instability in an environment of small stability to slantwise moist convection. Part I: Two-dimensional models, *J. Atmos. Sci.*, *44*(12), 1559–1573.
Frierson, D., I. Held, and P. Zurita-Gotor (2006), A gray-radiation aquaplanet moist GCM. Part I: Static stability and eddy scale, *J. Atmos. Sci.*, *63*, 2548–2566.
Fyfe, J. C. (2003), Extratropical Southern Hemisphere cyclones: Harbingers of climate change?, *J. Clim.*, *16*, 2802–2805.
Gilet, J., M. Plu, and G. Rivière (2009), Nonlinear baroclinic dynamics of surface cyclones crossing a zonal jet, *J. Atmos. Sci.*, *66*(10), 3021–3041.
Graff, L. S., and J. H. LaCasce (2014), Changes in cyclone characteristics in response to modified SSTs, *J. Clim.*, *27*, 4273–4295.
Hawcroft, M., H. Dacre, R. Forbes, K. Hodges, L. Shaffrey, and T. Stein (2016a), Using satellite and reanalysis data to evaluate the representation of latent heating in extratropical cyclones in a climate model, *Clim. Dyn.*, *48*, 2255–2278.
Hawcroft, M. K., L. C. Shaffrey, K. I. Hodges, and H. F. Dacre (2016b), Can climate models represent the precipitation associated with extratropical cyclones?, *Clim. Dyn.*, *47*, 679–695.
Hodges, K. I. (1995), Feature tracking on the unit sphere, *Mon. Weather Rev.*, *123*(12), 3458–3465.
Hodges, K. I. (1999), Adaptive constraints for feature tracking, *Mon. Weather Rev.*, *127*(6), 1362–1373.
Hoskins, B. J., M. E. McIntyre, and A. W. Robertson (1985), On the use and significance of isentropic potential vorticity maps, *Q. J. R. Meteorol. Soc.*, *111*, 877–946.
Kaspi, Y., and T. Schneider (2013), The role of stationary eddies in shaping midlatitude storm tracks, *J. Atmos. Sci.*, *70*, 2596–2613.
Kidston, J., S. M. Dean, J. A. Renwick, and G. K. Vallis (2010), A robust increase in the eddy length scale in the simulation of future climates, *Geophys. Res. Lett.*, *37*, L03806, doi:10.1029/2009GL041615.
Kodama, C., and T. Iwasaki (2009), Influence of the SST rise on baroclinic instability wave activity under an aquaplanet condition, *J. Atmos. Sci.*, *66*, 2272–2287.
Kushner, P. J., and L. M. Polvani (2006), Stratosphere-troposphere coupling in a relatively simple AGCM: Impact of the seasonal cycle, *J. Clim.*, *19*, 5721–5727.
Lackmann, G. M. (2002), Cold-frontal potential vorticity maxima, the low-level jet, and moisture transport in extratropical cyclones, *Mon. Weather Rev.*, *130*(1), 59–74.
Lambert, S. J., and J. C. Fyfe (2006), Changes in winter cyclone frequencies and strengths simulated in enhanced greenhouse warming experiments: Results from the models participating in the IPCC diagnostic exercise, *Clim. Dyn.*, *26*, 713–728.
Levine, X. J., and T. Schneider (2011), Response of the Hadley circulation to climate change in an aquaplanet GCM coupled to a simple representation of ocean heat transport, *J. Atmos. Sci.*, *68*, 769–783.
Lorenz, D. J., and E. T. DeWeaver (2007), Tropopause height and zonal wind response to global warming in the IPCC scenario integrations, *J. Geophys. Res.*, *112*, D10119, doi:10.1029/2006JD008087.

Lu, J., G. A. Vecchi, and T. Reichler (2007), Expansion of the Hadley cell under global warming, *Geophys. Res. Lett.*, *34*, L06805, doi:10.1029/2006GL028443.
Lu, J., G. Chen, and D. M. W. Frierson (2010), The position of the midlatitude storm track and eddy-driven westerlies in aquaplanet AGCMs, *J. Atmos. Sci.*, *67*, 3984–4000.
Mbengue, C., and T. Schneider (2013), Storm track shifts under climate change: What can be learned from large-scale Dry dynamics, *J. Clim.*, *26*, 9923–9930.
O'Gorman, P. A., and T. Schneider (2008), The hydrological cycle over a wide range of climates simulated with an idealized GCM, *J. Clim.*, *21*, 3815–3832.
Oruba, L., G. Lapeyre, and G. Rivière (2013), On the poleward motion of midlatitude cyclones in a baroclinic meandering jet, *J. Atmos. Sci.*, *70*(8), 2629–2649.
Pedlosky, J. (1987), *Geophysical Fluid Dynamics*, Springer, New York.
Pfahl, S., and M. Sprenger (2016), On the relationship between extratropical cyclone precipitation and intensity, *Geophys. Res. Lett.*, *43*, 1752–1758, doi:10.1002/2016GL068018.
Pfahl, S., P. A. O'Gorman, and M. S. Singh (2015), Extratropical cyclones in idealized simulations of changed climates, *J. Clim.*, *28*, 9373–9392.
Posselt, D. J., and J. E. Martin (2004), The effect of latent heat release on the evolution of a warm occluded thermal structure, *Mon. Weather Rev.*, *132*(2), 578–599.
Riviére, G. (2011), A dynamical interpretation of the poleward shift of the jet streams in global warming scenarios, *J. Atmos. Sci.*, *68*(6), 1253–1272.
Rossby, C. (1948), On displacements and intensity changes of atmospheric vortices, *J. Mar. Res.*, *7*, 175–187.
Son, S.-W., L. M. Polvani, D. W. Waugh, H. Akiyoshi, R. Garcia, D. Kinnison, S. Pawson, E. Rozanov, T. G. Shepherd, and K. Shibata (2008), The impact of stratospheric ozone recovery on the Southern Hemisphere westerly jet, *Science*, *320*, 1486–1489.
Stoelinga, M. T. (1996), A potential vorticity-based study of the role of diabatic heating and friction in a numerically simulated baroclinic cyclone, *Mon. Weather Rev.*, *124*(5), 849–874.
Tamarin, T., and Y. Kaspi (2016), The poleward motion of extratropical cyclones from a potential vorticity tendency analysis, *J. Atmos. Sci.*, *73*, 1687–1707.
Tamarin, T., and Y. Kaspi (2017a), Mechanisms controlling the downstream poleward deflection of midlatitude storm tracks, *J. Atmos. Sci.*, *74*, 553–572.
Tamarin, T., and Y. Kaspi (2017b), Enhanced poleward propagation of storms under climate change, *Nat. Geosci.*, doi:10.1038/s41561-017-0001-8.
Ulbrich, U., J. G. Pinto, H. Kupfer, G. C. Leckebusch, T. Spangehl, and M. Reyers (2008), Changing Northern Hemisphere storm tracks in an ensemble of IPCC climate change simulations, *J. Clim.*, *21*, 1669–1679.
Wu, Y., M. Ting, R. Seager, H.-P. Huang, and M. A. Cane (2011), Changes in storm tracks and energy transports in a warmer climate simulated by the GFDL CM2.1 model, *Clim. Dyn.*, *37*, 53–72.
Yettella, V., and J. E. Kay (2016), How will precipitation change in extratropical cyclones as the planet warms? Insights from a large initial condition climate model ensemble, *Clim. Dyn.*,1–17, doi:10.1007/s00382-016-3410-2.
Yin, J. H. (2005), A consistent poleward shift of the storm tracks in simulations of 21st century climate, *Geophys. Res. Lett.*, *32*, L18701, doi:10.1029/2005GL023684.
Zappa, G., L. C. Shaffrey, and K. I. Hodges (2013), The ability of CMIP5 models to simulate North Atlantic extratropical cyclones, *J. Clim.*, *26*, 5379–5396.